### PROCEEDINGS OF SPIE

SPIEDigitalLibrary.org/conference-proceedings-of-spie

# Label-free alternating-current plasmonic nanopore sensing of nanoparticles

Renkes, Scott, Kim, Minjun, Alexandrakis, George

Scott Renkes, Minjun Kim, George Alexandrakis, "Label-free alternating-current plasmonic nanopore sensing of nanoparticles," Proc. SPIE 11978, Plasmonics in Biology and Medicine XIX, 1197808 (3 March 2022); doi: 10.1117/12.2607884



Event: SPIE BiOS, 2022, San Francisco, California, United States

## Label-free alternating-current plasmonic nanopore sensing of nanoparticles

Scott Renkes<sup>a</sup>, Minjun Kim<sup>b</sup>, and George Alexandrakis<sup>a</sup>

<sup>a</sup>University of Texas at Arlington, Bioengineering Department, Arlington, TX, USA <sup>b</sup>Southern Methodist University, Department of Mechanical Engineering, Dallas, TX, USA

#### ABSTRACT

Alternating current (AC) modulation of command voltage applied across a Self-induced Back Action Actuated Nanopore Electrophoresis (SANE) sensor, a type of plasmonic nanopore sensor that we have developed previously, enables acquisition of new data types that could potentially enhance the characterization of nanoparticles (NPs) and single molecules. In particular, AC voltage frequency response provides insight into the charge and dielectric constant of analytes that are normally obfuscated using DC command voltages. We first analyzed Axopatch 200B data to map the frequency response of the empty SANE sensor in terms of phase shift and amplitude modulation, with and without plasmonic excitation. We then tested the frequency response of 20 nm diameter silica NPs and 20 nm gold NPs trapped optically, which made these particles hover over an underlying 25 nm nanopore at the center of the SANE sensor. By applying a DC command voltage with a superimposed AC frequency sweep while keeping the NPs optically trapped in the vicinity of the nanopores's entrance, we have found that silica and gold NPs to have distinctly different electrical responses. This pilot work demonstrates the feasibility of performing AC measurements with a plasmonic nanopore, which encourages us to pursue more detailed characterization studies with NPs and single molecules in future work.

**Keywords:** plasmonics, nanopores, nanoparticles, alternating current, SANE sensor

#### 1. INTRODUCTION

Nanopores are commonly used to discriminate between analytes through the analysis of changes in conduction current profiles during translocation. Nanopore measurements have enabled discrimination between single molecule species in solution,<sup>1</sup> attained low-cost and label-free DNA sequencing,<sup>2,3</sup> with additional possible applications expanding rapidly.<sup>4,5</sup> However, the translocation times of analytes through a traditional nanopore are extremely fast, which limits the fidelity of electrical data that can be collected. Through the use of optical trapping enabled by the self-induced back-action (SIBA) effect, nanopores can be enhanced not only by slowing down the translocation of analytes, but also by introducing new dimensionality to the collected data through the collection of optical data simultaneously with electrical data.<sup>6,7</sup> To that end, we previously developed a SIBA actuated nanopore electrophoresis (SANE) sensor, effectively a nanopore with plasmonic optical trapping, which has been shown capable of trapping individual nanoparticles (NPs), proteins and protein complexes<sup>8</sup> and through the use of bimodal optical and electrical data can discriminate between analyte species.<sup>6,9,10</sup>

Here we propose that additional data can be collected by driving the SANE sensor with an AC voltage. Use of AC sensing has been inaccessible to traditional nanopore research due to fast translocation times, typically in the hundreds of  $\mu$ s, <sup>11,12</sup> which would necessitate a MHz driving frequency that exceeds the frequency limit of the most common, currently used instrumentation amplifiers for nanopore research. The optical trap of the SANE sensor provides trapping duration in the seconds range, <sup>6,13</sup> which allows for frequencies as low as 1 Hz. The upper bound of possible AC measurement frequencies is currently set by the amplifier hardwired filters (100 kHz) and the data acquisition sample rate (500 kHz).

Further author information: (Send correspondence to Scott Renkes)

G.A.: E-mail: galex@uta.edu, Telephone: 1 817 272 3496

S.R.: E-mail: sar9179@mavs.uta.edu, Telephone: 1 740 272 6710

Plasmonics in Biology and Medicine XIX, edited by Tuan Vo-Dinh, Ho-Pui A. Ho, Krishanu Ray, Proc. of SPIE Vol. 11978, 1197808 · © 2022 SPIE · 1605-7422 · doi: 10.1117/12.2607884

Two possible uses of AC-based characterization of optically trapped analytes come to mind. First, by introducing AC frequency modulation, the mobility of ions in the fluid around analytes will depend on analyte surface charge, and material properties in the case of NPs, thus possibly enhancing the capacity of the sensor to distinguish between analyte species. Second, AC modulation could enable current to travel through a NP, thus enabling improved characterization of drug delivery and gene therapy vehicle preparations. This work presents initial tests of the first of these aforementioned uses of AC sensing through pilot measurements for discriminating between 20 nm silica  $(SiO_2)$  and 20 nm gold (Au) NPs.

#### 2. METHODS

We started with an experimental system described in Raza et. al.<sup>6</sup> that uses a 820 nm near-infrared laser diode (L820P200, Thorlabs, Newton, NJ) that has its polarization adjusted to match the orientation of the sensor's narrow waist, where plasmonic enhancement is the strongest. The optical data was collected by a photodiode that recorded the transmitted light intensity through the sensor, which increased in a stepwise manner when a NP was trapped and then stepwise decreased when the NP translocated through the sensor. Electrical data consisting of a positive current spike when the NP entered the optical trap, current fluctuations while the particle stayed in the trap, and a negative spike when the NP escaped the trap and translocated through the immediately underlying nanopore, were collected synchronously using an Axopatch 200B system (Molecular Devices, San Jose, CA) and all data was digitized using an Axon Digidata 1440 ADC (Molecular Devices). For the AC measurements, the optical data was also sent to an Arduino Uno (Adafruit Industries, New York, NY) programmed to perform edge detection, looking for an optical step change indicative of a trapping event, which was accompanied by a simultaneous current spike in the electrical data stream. The Arduino then sent a trigger to an Agilent 33250A Waveform/Function Generator (Agilent Technologies, Santa Clara, CA) that generated a user-defined pulse at a selected frequency and amplitude. The function generator set the command voltage for the Axopatch 200B, which was operated in voltage clamp mode. The ratio of measured current amplitude to command voltage, i.e. conductance, was computed as a characteristic parameter of the NP response to the AC modulation, that we will refer to as an AC burst event. Furthermore, fast-Fourier transform (FFT) analysis of the recorded AC signal responses enabled calculating the phase change while the particle was driven by the AC burst. Additional data types were obtained from fitting post-drive decay data, once the driving burst had stopped, to an empirically derived formula incorporating a damped oscillation term, as described below. The DC voltage was consistently on and kept at 100 mV (-ve cis to +ve cis) for all experiments.

A baseline AC response was established using a model cell reference block provided by the Axopatch 200B manufacturer for calibrating the system. The model cell bath, that has an equivalent circuit of a 10 M $\Omega$  resistor in series with a 4 pF capicitor, was used for impedance matching during these baseline measurements with the Axopatch 200B. Each sensor that was used in the AC measurements was also baselined using 40  $\mu$ L of 0.3 M KCl solution at 7.4 pH. Baseline measurements were performed at 110 mV command voltage with one of the following AC frequencies superimposed: 1, 2, 5, 10, 20, 50, 100, 1k, 2k, 5k, 10k, 20k, 50k and 80k Hz. Modulation at higher frequencies was not possible with our experimental setup due to a hard-wired Bessel filter in the Axopatch 200B system with a maximum cutoff frequency of 100 kHz. The amplitude of the waveform at each frequency was set to ensure there was a high signal to noise ratio but low enough to ensure the Axopatch 200B did not saturate while recording the current response. 1 Hz measurements were taken with a 10 Vp-p signal and 1 kHz were generally collected at 50 mVp-p. The Axopatch 200B front-switched command voltage port was used to connect to the function generator. This port reduced all signals by a factor of 20. Each frequency was set to pulse 5 times with 10 cycles each to enable testing the reproducibility of the response. In addition, signal decays recorded at the end of each burst were analyzed to generate additional data types for the characterization of NPs.

The  $20 \pm 4$  nm  $SiO_2$  NPs (MEL0010, NanoComposix, zeta potential = -40 mV) and  $20 \pm 2$  nm Au NPs (C11-20-TM-DIH-50, Nanopartz, zeta potential= -15 mV) were selected as the analytes to study in this pilot work because both NPs have been well characterized in our previous work with DC SANE sensor measurements.<sup>6</sup> The  $SiO_2$  NPs were used to characterize the system response to dielectric materials and the Au particles were used to show the response of conductive materials and their response were expected to be different. The  $SiO_2$  NPs were tested at the same frequencies as the baseline measurement for comparison with the empty trap response

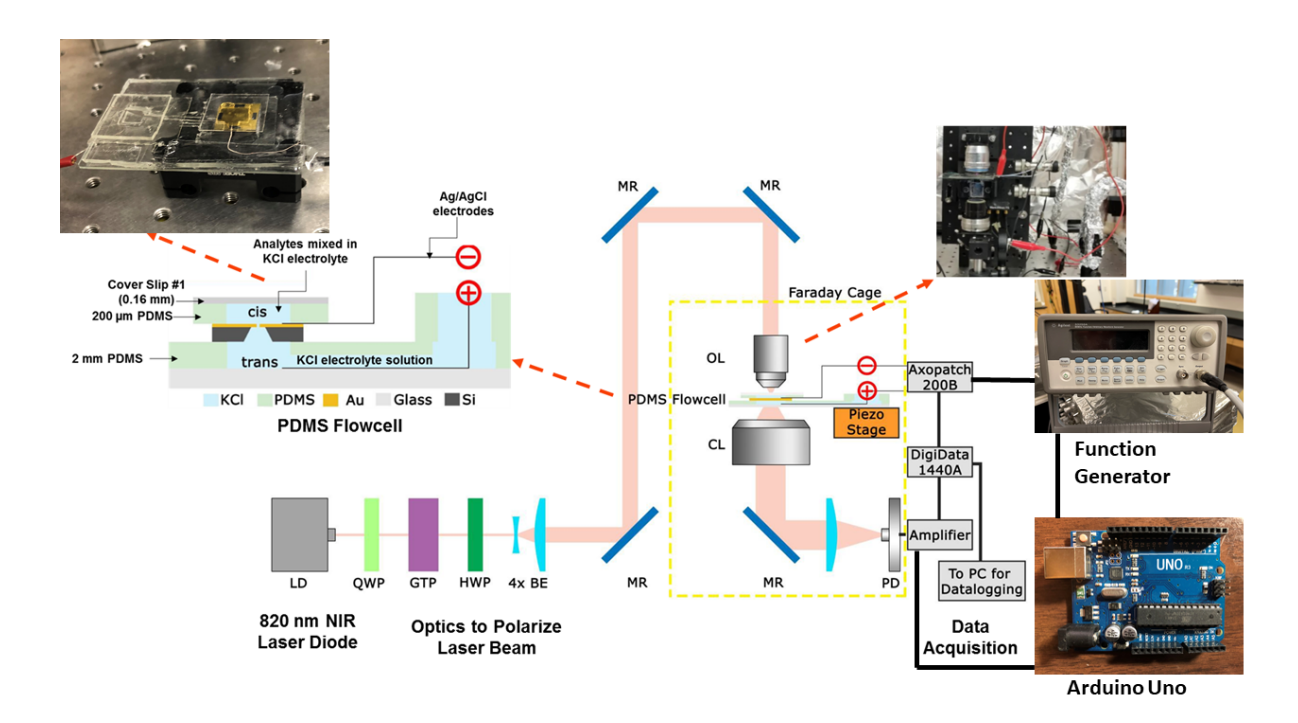


Figure 1. Complete experimental setup including flow cell, optical setup and data acquisition equipment. A detailed description of the setup can be found in Raza et. al.<sup>6</sup> The Arduino Uno and Agilent function generator were added to the experimental setup to provide optical-based triggering for the function generator and AC pulsed oscillation command signals to the Axopatch 200B.

and model cell response. We also performed post-decay analyses after driving the NP in the trap at a single frequency of 100 Hz. The Arduino was programmed to trigger an AC burst on both a positive and negative optical step change to ensure a trapping event AC burst was paired to a non-trapping burst event.

Once the data was collected, each pertinent AC burst event was noted for start and stop times as well as if it took place during a trapping event or not. The event parameters were imported into a MongoDB document database (MongoDB Inc, New York, NY) and then loaded into Matlab (MathWorks, Natick, MA) to first be processed for frequency response and then for decay response. The axon binary file (.abf) generated by the pCLAMP software (Molecular Devices) was trimmed according to the event times and an FFT was performed on the current response and command voltage of the .abf data as depicted in Fig. 2. The center frequency of the oscillation was determined by the FFT and was then used to identify the phase difference between the command voltage and the current response. The magnitudes of peak amplitude, with both current response and command voltage, were divided to calculate conductance of the sensor during the AC burst event. The phase change at each frequency for the model cell was subtracted from the empty trap to determine the sensor specific phase change. The conductance at each frequency for the empty trap was divided by the model cell conductance to produce a ratio of conductance to calculate conductance response specific to the sensor. In a similar manner, the phase change of the empty trap was subtracted from the phase change of 1 fM  $SiO_2$  at each frequency to look at the phase change relative to the empty sensor response. The conductance ratio was calculated at each frequency by dividing the sensor conductance for 1 fM  $SiO_2$  by the empty trap conductance.

Next, the data was processed for their post-drive decay profiles. The updated event parameters were loaded back into Matlab where the pCLAMP data was trimmed at the termination of the AC pulse by smoothing the command voltage and then taking the first derivative to determine where along the time-axis the signal returned to the DC baseline voltage. The event time was then extended by 3 ms and by using the prepareCurveData() and fit() functions in Matlab with the "NonlinearLeastSquares" option, and the decay profile was fit using Eq. 1. The form of this equation was selected empirically as the sum of a damped oscillation, representing the

particle's decaying oscillation, and a line with a negative slope, representing particle drift (Eq. 1. The initial fitting parameters were set accordingly: a1 and a2 were set to the minimum absolute value of the trimmed data segment, b1 was set to the maximum absolute value of the trimmed data segment, c1 was set emperically to 15000 for  $SiO_2$  NPs, 10000 for Au NPs and empty trap, d1 was set to 0 and e1 was set empirically to 0.653. The  $R^2$  value of the fit was used to filter out poorly fitting data (threshold set a 0.9) and the remaining parameters were analyzed to see how the NP type and concentrations would affect the post-drive decay parameters.

| Parameter | Empty      | Au         | $50 \text{ fM } SiO_2$ | $1 \text{ fM } SiO_2$ |
|-----------|------------|------------|------------------------|-----------------------|
| a1        | signal min | signal min | signal min             | signal min            |
| a2        | signal min | signal min | signal min             | signal min            |
| b1        | signal max | signal max | signal max             | signal max            |
| c1        | 10000      | 10000      | 11636                  | 5000                  |
| d1        | 0          | 0          | 0                      | 0                     |
| e1        | 0.635      | 0.635      | 0.635                  | 0.635                 |

Table 1. Initial parameters used to fit Eq. 1

$$y = a1 + a2 * x + b1 * sin(c1 * x + d1) * e^{e1 * x}$$
(1)

All the experiments shown in this work were performed with a single sensor to allow for easy comparison between different experiments. This sensor was fabricated in-house at the Shimadzu Institute Nanotechnology Research Center (Arlington, TX) and Ne/He focused ion beam milling, to generate the optical trap and nanopore parts of the sensor, was performed at Oak Ridge National Laboratory (CNMS, Oak Ridge, TN).

#### 3. RESULTS

We began our experiments by performing a baseline measurement of the model cell and then with the SANE sensor with 0.3 M KCl load and an empty trap. The results of the baseline experiments are presented in Fig. 3. Although optical transmission appeared unaffected by the AC drive (data not shown) significant phase and conductance changes were noted as a function of frequency. After subtracting the model cell phase response from that of the empty sensor, a biphasic phase dependence became obvious with a point of inflection around zero net phase change for the sensor, around 1 kHz. Also, once the model cell conductance response was divided out from the empty sensor, a peak in empty sensor conductance was also noted around 1 kHz. The phase shift leveled out around 5 kHz and then started decreasing with increasing driving frequency, while the conductance ratio dropped back with a point of inflection around 2 kHz. A pre-peak point of infection was also noted at about 200 Hz.

In order to avoid multi-particle interactions in the vicinity of the optical trap we ran experiments using ultralow concentrations of 1 fM solution of  $SiO_2$  NPs at the same frequencies used for the baseline and compared them to the response of the empty trap, corrected for model cell response. The largest change in phase was seen at 1 kHz (Fig. 4a), which coincided with the point of inflection in the phase change increase of the empty trap, near its zero-phase response, shown in Fig. 3a. The relative conductance decreased with driving frequency with a point of inflection around 1 kHz, where NP phase response was maximum. In addition, a secondary maximum was seen around 5 kHz (Fig. 3b).

In addition to doing a frequency scan, both  $SiO_2$  and Au NPs were driven at 100 Hz, in this pilot work to compare their relative phase shift (Fig. 4c) and conductance (Fig. 4d) responses, each at two different concentrations, relative to the empty sensor response. The Au NP increased the conductance of the sensor chip and increased it even more at the higher concentration. In contrast, the  $SiO_2$  conductance increase relative to the empty sensor was lower and reduced with increasing NP concentration. In terms of phase change relative to the empty sensor, the  $SiO_2$  dielectric NPs showed a stronger response than the conducting Au particles that had values near to those of the empty sensor. Interestingly, the Au NPs' phase shift appeared to show no strong concentration

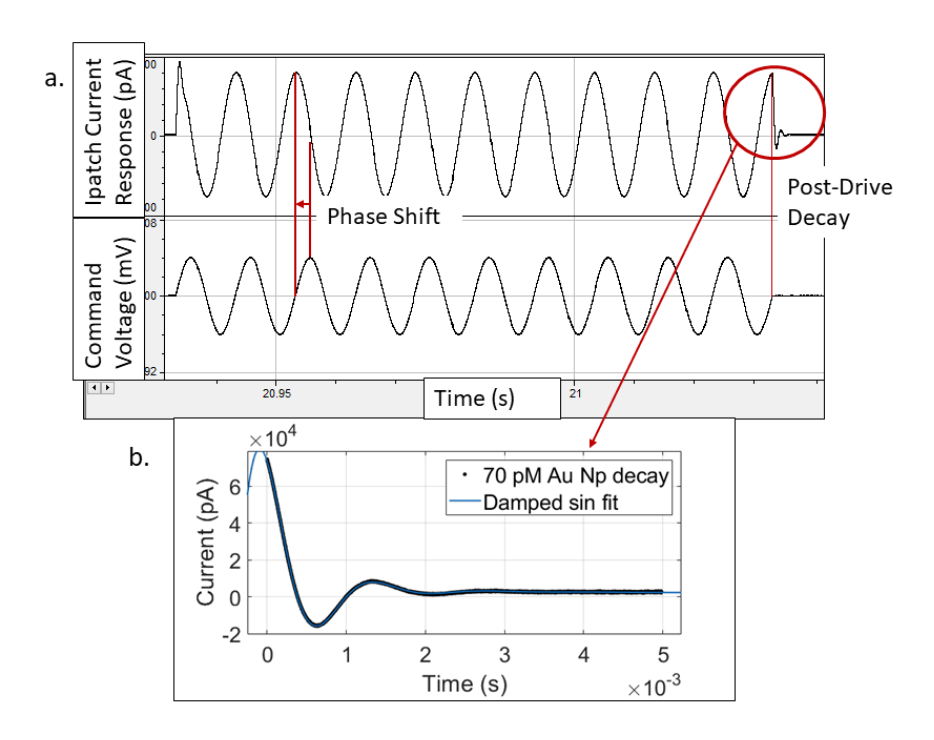


Figure 2. a. Example of 100 Hz AC oscillation during a 70 pM Au NP run. Phase shift was calculated from taking the difference of the command voltage phase and the measured current response phase. A negative phase indicates a phase lag of the current response. b. An example fit of the 70 PM post-drive decay with an  $R^2 > 0.99$ , representing a good fitting result. The damped oscillation was fit to the post-drive decay that was trimmed at the termination of the command voltage oscillation.

dependence, whereas the  $SiO_2$  NPs showed a strong one (Fig. 4d). However, when tested using a Wilcoxon rank sum test, we obtained a p-value of 0.002, so we would reject the null hypothesis for a 0.05 level of significance and conclude that the mean phase shift for the two Au NP solutions did have a concentration-dependent phase shift.

Subsequently, we examined the post-drive decay that was fitted to damped oscillation riding on a linear slope, according to Eq. 1. Any fit with an  $R^2$  value less than 0.9 was excluded from the analysis to mitigate the effect of noisier measurements on fit parameters. The 100 Hz pulse post-drive decay parameters of the fit to Eq. 1 are presented in Fig. 5. Figs. 5a and 5d show that the intercept and slope, respectively, of the linear component of the drift have both particle-type and concentration-based dependence. In contrast, the empty trap rested at zero-intercept and at flat slope, indicating that any post-drive linear drift was the result of NP interactions with the applied AC bias. Fig. 5b shows the magnitude of the periodic component of the damped oscillation. This factor was dependent on analyte type, though the amplitude of the oscillation was largely independent of each NP type's concentration. Furthermore, there were several outliers on the 50 fM  $SiO_2$  run shown in Fig. 5b with  $R^2$  fit values above 0.9. We do not currently know the cause for these outliers, but we are actively exploring sources of possible measurement bias, or if in fact a physical explanation exists. Fig. 5c shows the frequency of the post-drive damped oscillation, which was much higher than the driving frequency of 100 Hz. The empty sensor had the highest natural decay frequency, while the loaded sensor measurements showed both a NP type and concentration dependence in that frequency. The Au NPs had a higher frequency than the  $SiO_2$  NPs and were closer to the decay frequency of the empty sensor than  $SiO_2$  ones. In addition, the decay frequency relationship with concentration was inverse between Au versus  $SiO_2$  NPs, where the former had decreased frequency and the latter increased frequency with increasing concentration. Interestingly, the outliers of the 50 fM  $SiO_2$  in Fig. 5c

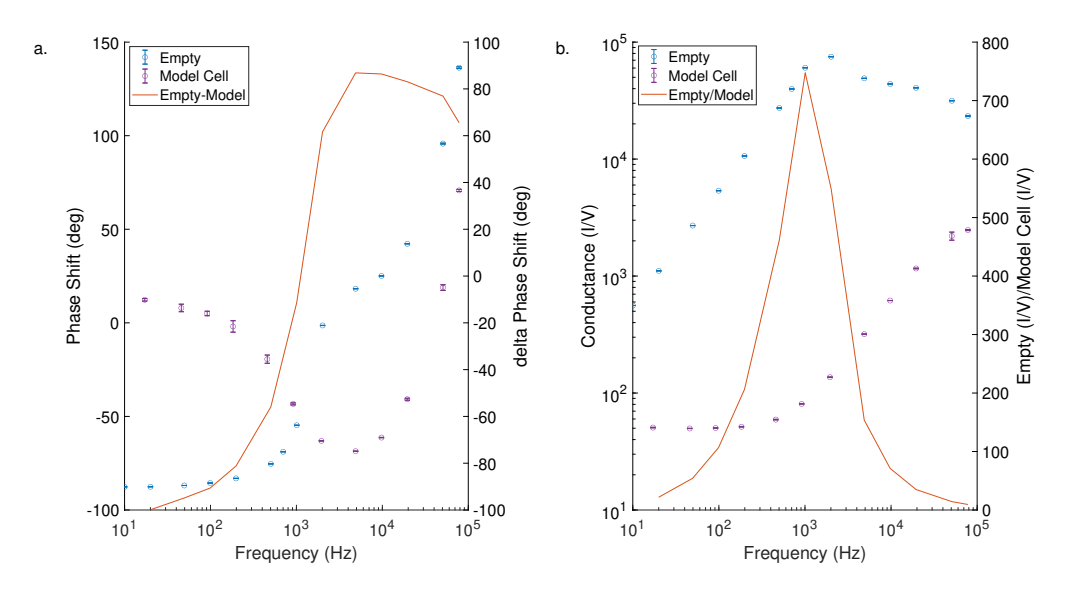


Figure 3. a. Phase shift plot of empty trap and model cell response. Phase shift was calculated as described in Fig. 2. The right axis plot show the phase difference between empty sensor and model cell, representing the true response of the empty sensor (orange curve). b. The conductance of the sensor was calculated by dividing the current response (pA) by the command voltage (mV) at peak oscillation values. The right axis plot show the ratio of the empty trap response to the model cell response intended to remove the effect of the system response from the sensor response (orange curve).

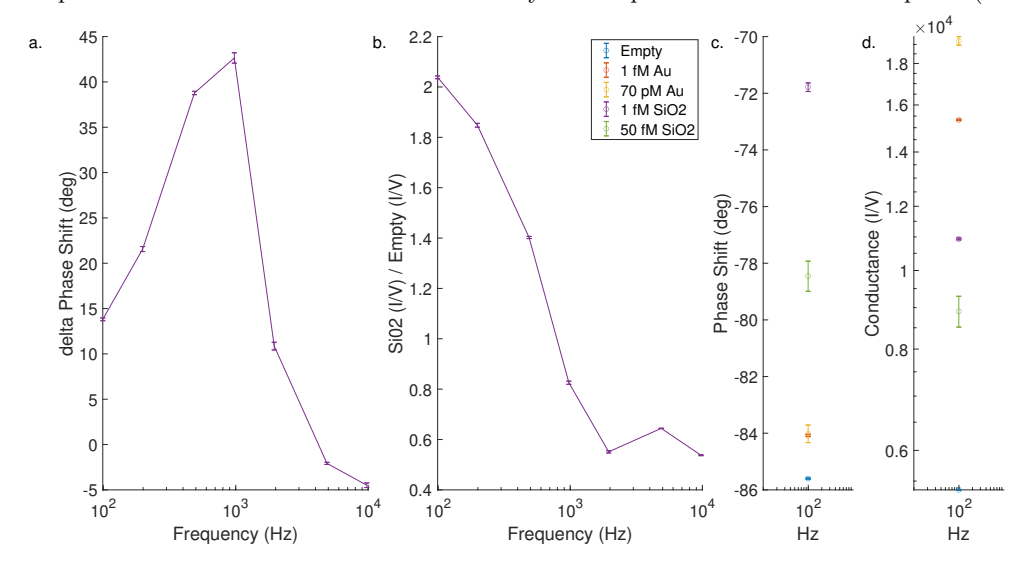


Figure 4. a. Difference of 1 fM  $SiO_2$  NP phase response and empty trap phase response at 100 Hz driving frequency. b. Ratio of 1 fM  $SiO_2$  NP conductance and empty trap conductance. c. Conductance and d. Phase response of  $SiO_2$  and Au NP solutions and of the empty trap at 100 Hz driving frequency.

have similar frequency with the main grouping of frequency responses for the 1 fM concentration (red oval). Fig. 5e shows the phase response of the damped oscillation. The response of Au NP solutions coincided with that of the empty trap that is also made of Au. In contrast, the  $SiO_2$  NPs had a distinct phase shift and also showed a decreasing phase shift with increasing concentration. Similar to the decay frequency, the outliers of the higher  $SiO_2$  concentration solution correlates with the group-wise values of the lower concentration solution (red oval). Finally, Fig. 5f shows the decay exponent for the envelope of the damped oscillation. This panel tells a more complex story. The empty trap response was between the response of the two NP solutions. The concentration dependence was not as pronounced but there were distinct differences between the particle types.

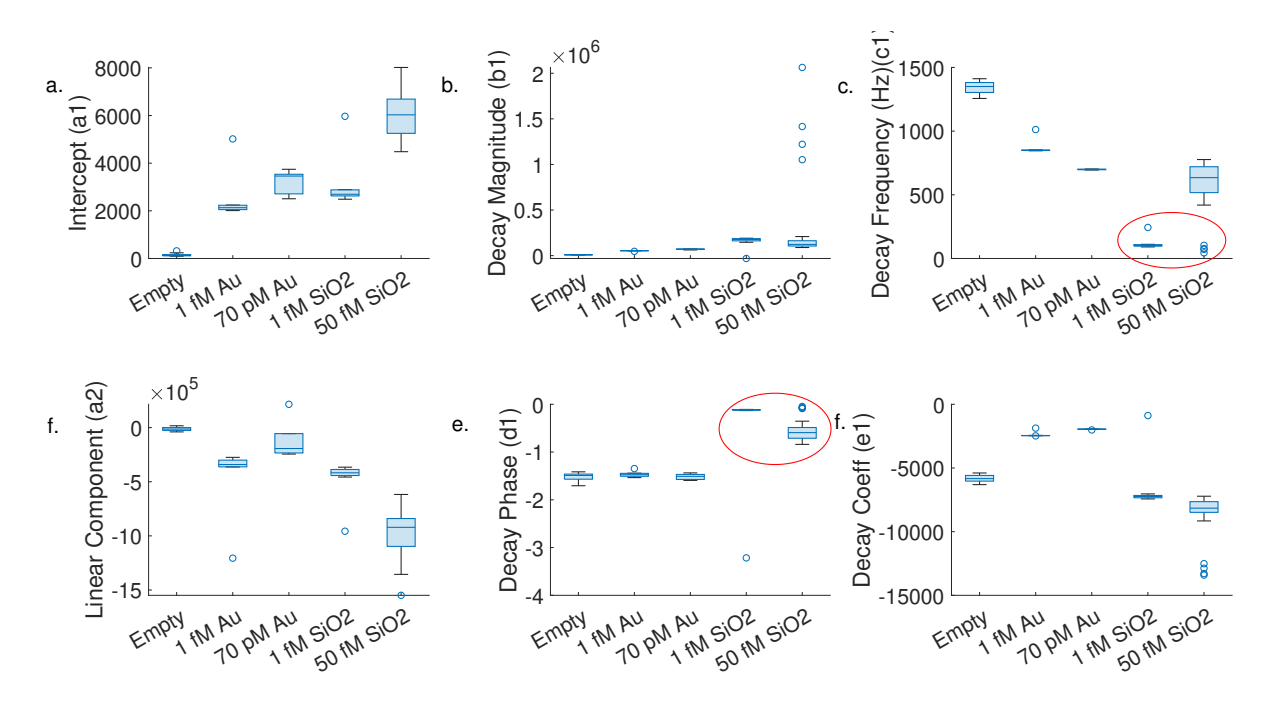


Figure 5. Damped oscillation fit parameters of Eq. 1,  $y = a1 + a2 * x + b1 * sin(c1 * x + d1) * e^{c1 * x}$  a. Intercepts of regression (a1) for  $SiO_2$  and Au NPs and the empty sensor. a. Intercepts of regression (a1), b. Magnitude of oscillation for regression (b1), c. Frequency response of post-drive decay (c1), d. Slope of linear drift component (a2), e. Post-drive decay oscillation phase (d1), and f. Decay coefficient for the damped oscillation envelope (e1). Red ovals in c. and e. highlight the similarity of a minority of  $SiO_2$  NP responses at the higher concentration to the majority of those at the lower concentration.

#### 4. DISCUSSION

The function selected to fit the post-drive decay (Eq. 1) was selected empirically by inspection of curves similar to the one shown in Fig. 2a. Addition of the linear component brought  $SiO_2$  fits from an 0.85  $R^2$  value to above 0.9, many hitting 0.99. The fitting parameter initial guesses were chosen empirically to provide consistently good quality fits (Table 1). Some sensitivity in fitting results to initial guesses was observed.

The baseline analysis that created Fig. 3 suggested the presence of a resonant response for the empty sensor that was reminiscent to that of a resistive-capacitive circuit, <sup>14</sup> with 1 kHz as the resonant frequency. In future work, we will expand the frequency sweep further toward the 100 kHz Bessel filter of the Axopatch to test for the presence for any other possible resonance structure at higher frequencies. The baseline analysis can also provide insight into what frequencies should be used to maximize sensor response sensitivity. To that end, in near future work we will also perform denser sampling of the frequencies around 1 kHz to identify the optimal operating frequency more accurately.

The  $SiO_2$  NP frequency response (Fig. 4a) confirmed that a driving frequency in the vicinity of 1 kHz would be near the SANE sensor's highest sensitivity response. In that frequency range the phase difference between the  $SiO_2$  NP and the empty sensor was the largest. In fact, the sensor's phase response was near zero at that frequency, which defined the point of inflection between negative and positive phase responses (Fig. 3a). In contrast, although the empty sensor had a conductance maximum in the 1 kHz range (Fig. 3b), the  $SiO_2$ presence acted as a low-pass filter on the sensor (Fig. 4b). In near future work we will expand the frequency spectrum for  $SiO_2$  NPs to confirm whether the minimum seen in Fig. 4b is a local or a global minimum.

For the driven oscillation at 100 Hz, the highest conductance was seen by the Au NPs and more so of the higher concentration. In contrast,  $SiO_2$  NPs showed a lower conductance than the Au NPs, but still higher than that of the empty sensor. The difference in conductance increase between Au and  $SiO_2$  NPs can be justified by the fact that Au is a conductor that would oppose changes in the applied voltage bias, which would in turn cause

ionic fluid motion around these particles. On the other hand,  $SiO_2$  NPs are dielectric and would polarize in the presence of the AC field, which would augment ionic charge displacement relative to an empty sensor, but less so than the conducting Au NPs. Another important factor to consider is that particles are likely to accumulate over the SANE sensor because they are driven there by the DC bias, but then they cannot easily tunnel through the optical trap.<sup>10</sup> This results in a 'traffic jam' of NPs that may all feel the effects of the applied AC bias. We speculate it is for this reason that the phase response for  $SiO_2$  NPs in Fig. 4d is lower at the higher concentration, as NPs may experience different field strengths depending on their position and may collide with each other, which would contribute to decoherence of phase. On the other hand, the Au NPs resist the applied AC bias near-instantaneously and collectively increase the detected conductance at higher concentrations (Fig. 4d).

Next, we consider the SANE sensor derived parameters from the post-drive signal decay profiles. The larger amplitude line intercept and the steeper linear slope superimposed onto the post-drive decay at 100 Hz (Figs. 5a and 5d, respectively) could provide some insight into the charging effects of the  $SiO_2$  NPs: Once the driven oscillation has ceased at the peak point of the AC oscillation the  $SiO_2$  NP may hold a surface charge that needs to decay back to the DC baseline state. This effect is more pronounced at higher  $SiO_2$  NP concentrations as the particles that had accumulated near the mouth of the pore all others above it contributed to different degrees, depending on their position, to this discharging effect. In contrast, Au NP's did not have this sloping response as, being conductors, could adjust their surface to the applied field very quickly.

The decay magnitude in Fig. 5b likely provides similar insight as the intercept (Fig. 5a) and hints at the higher charge stored on the  $SiO_2$  NPs at the peak of the AC drive. The outliers present in Fig. 5b raise some questions as to why the oscillation magnitude spikes by almost an order of magnitude larger sometimes without drastically reducing the  $R^2$  of the fit function. In the near future we will perform careful additional experiments to identify the experimental conditions under which those outliers show up.

The decay frequency of post-drive oscillations, shown in Fig. 5c demonstrates natural decay frequencies for the empty sensor and all NPs that were much higher than the 100 Hz driving oscillation. Also, a clear dependence on NP concentration. It is interesting that the decay frequency for Au NPs was somewhat lower for the higher concentration, whereas in the case of  $SiO_2$  NPs was higher for the higher concentration. This parameter bears further investigation to identify what determines this frequency dependence. We speculate that this phenomenon may be related to charging effects: Au NPs can adjust quickly to the external field and interaction of the NP inside the optical trap with ones above it the ensemble could be moving like a heavier 'particle', which would result in a lower resonant frequency, as per Hooke's law. On the other hand,  $SiO_2$  NPs are charged up at the end of the driving cycle, which may affect the balance between the electrophoretic, dielectrophoretic, electroosmotic and optical trapping forces and, in turn, the stiffness of the apparent spring constant for this trap. Another possibility related to a concentration dependent effect is a packing effect. Ludwig et. al. 15 observed two different performance scaling laws depending on the packing density of  $SiO_2$ . A likely localized high concentration observed by Peri et. al. 10 could be occurring near the trap in the 50 fM  $SiO_2$  solution resulting in the dense packing of  $SiO_2$  NP causing the difference in frequency response from the 1 fM  $SiO_2$  solution.

Fig. 5e is a great illustration of what was seen in Fig. 4d applied to a different harmonic motion. The  $SiO_2$  NPs have a much different phase shift from the Au NPs, which have a concentration independent response that is very close to the empty sensor one. The lower concentration of  $SiO_2$  also shows a larger phase shift than the higher concentration lending support to the idea that higher concentrations of  $SiO_2$  NPs reduces their oscillatory coherence by physical collisions. Of note, the outliers of the 50 fM concentration match the phase shift of the 1 fM concentration lending credence to the idea that we are seeing a localized concentration effect. Further study would be needed to characterize this phenomenon.

Finally, the decay coefficient in Fig. 5f serves to control as the damping envelope to the post-drive decay. It is interesting that the decay coefficient of Au NPs is less negative than that of the empty sensor, whereas the  $SiO_2$  NPs have a more negative one. One can imagine that the conducting Au NPs resist applied field changes and therefore are less affected by charging effects in their immediate environment as they come to a rest. On the other hand  $SiO_2$  particles are charged when the post-drive cycle begins and this engenders the presence of the electroosmotic forces that would oppose translocation with a magnitude that decreased as the NPs discharged.

The optical performance of the system did not provide any insight other than there was no optical response to the AC modulation of analytes. However, this does provide some insight into the stiffness of the optical trap and the direction of motion the particles experience. The majority of optical transmission change seen by the SANE sensor is due to particles entering and leaving the trap. When a particle enters the trap it serves as a dielectric lens and increases the intensity of light that is transmitted through the pore. If the AC modulation is causing a particle to oscillate in line with the nanopore without leaving the trap, it would likely not cause a noticeable change in the optical transmission. Neumeier et. al. 16 state that the time required for a particle to return to its favored state in the optical trap is on the order of pico-seconds. However, the particle must make its way through the trap in order for it to translocate and leave the trap. This could allow for inline movement of the NP while in the trap. We did not see any oscillations that conclusively resulted in a trapping or translocation event, so the force preventing a NP from leaving the trap was likely greater than the force of the driven oscillation.

#### 5. CONCLUSIONS

This work presents the first feasibility results for AC-driven plasmonic nanopore sensing. Our pilot findings suggest that AC measurements could discriminate between Au and  $SiO_2$  NPs of the same diameter. However, the model-deduced oscillation parameters, during and post-drive, both appeared to be concentration dependent. At the lower of the concentrations used for each particle type, the separation in values between particle types for a given oscillation parameter became more pronounced. We speculate that these types of AC measurements could be useful in the future for the characterization of biological NPs (liposomes, gene therapy vehicles) and drug delivery particles. However, analyte concentration would need to be optimized for each NP type to minimize the concentration dependence of measured phase and conductance, as this could in turn confound the interpretation of measurements in heterogeneous analyte solutions. Furthermore, once concentration optimization is achieved, we plan to expand this technique into medically-relevant proteins with the aim of enhancing the SANE sensor's capacity to differentiate between specific and non-specific binding events.

#### ACKNOWLEDGMENTS

We thank Dr. Karren L. More and Dr. Alex Belianinov for allowing us access and providing technical guidance on focused ion beam milling at the Center for Nanophase Materials Sciences (CNMS) at Oak Ridge National Laboratory (ORNL) in Oak Ridge, TN. We are also thankful to all the engineers and staff at the Shimadzu Institute Nanotechnology Research Center at the University of Texas at Arlington for their support and guidance. The authors acknowledge the financial support from the National Cancer Institute (1R21CA240220-01A1), the National Heart, Lung, and Blood Institute (NIH T32 HL134613) for Scott Renkes and the National Science Foundation (CBET#2022398 and CBET#2022374). The content is solely the responsibility of the authors and does not necessarily represent the official views of the National Institutes of Health.

#### REFERENCES

- [1] Lu, Y., Wu, X.-Y., Ying, Y.-L., and Long, Y.-T., "Simultaneous single-molecule discrimination of cysteine and homocysteine with a protein nanopore," *Chemical Communications* **55**(63), 9311–9314 (2019).
- [2] Jain, M., Olsen, H. E., Paten, B., and Akeson, M., "The oxford nanopore minion: delivery of nanopore sequencing to the genomics community," *Genome biology* **17**(1), 1–11 (2016).
- [3] Lee, J. S., Oviedo, J. P., Bandara, Y. M. N. D. Y., Peng, X., Xia, L., Wang, Q., Garcia, K., Wang, J., Kim, M. J., and Kim, M. J., "Detection of nucleotides in hydrated ssdna via 2d h-bn nanopore with ionic-liquid/salt-water interface," *Electrophoresis* 42(7-8), 991-1002 (2021).
- [4] Nehra, A., Ahlawat, S., and Singh, K. P., "A biosensing expedition of nanopore: a review," Sensors and Actuators B: Chemical 284, 595–622 (2019).
- [5] Lee, J. S., Saharia, J., Bandara, Y. N. D., Karawdeniya, B. I., Goyal, G., Darvish, A., Wang, Q., Kim, M. J., and Kim, M. J., "Stiffness measurement of nanosized liposomes using solid-state nanopore sensor with automated recapturing platform," *Electrophoresis* 40(9), 1337–1344 (2019).
- [6] Raza, M. U., Peri, S. S. S., Ma, L.-C., Iqbal, S. M., and Alexandrakis, G., "Self-induced back action actuated nanopore electrophoresis (sane)," *Nanotechnology* 29(43), 435501 (2018).
- [7] Verschueren, D., Shi, X., and Dekker, C., "Nano-optical tweezing of single proteins in plasmonic nanopores," Small Methods 3(5), 1800465 (2019).

- [8] Al Balushi, A. A. and Gordon, R., "Label-free free-solution single-molecule protein-small molecule interaction observed by double-nanohole plasmonic trapping," *ACS photonics* **1**(5), 389–393 (2014).
- [9] Peri, S. S. S., Sabnani, M. K., Raza, M. U., Ghaffari, S., Gimlin, S., Wawro, D. D., Lee, J. S., Kim, M. J., Weidanz, J., and Alexandrakis, G., "Detection of specific antibody-ligand interactions with a self-induced back-action actuated nanopore electrophoresis sensor," *Nanotechnology* **31**(8), 085502 (2019).
- [10] Peri, S. S. S., Sabnani, M. K., Raza, M. U., Urquhart, E. L., Ghaffari, S., Lee, J. S., Kim, M. J., Weidanz, J., and Alexandrakis, G., "Quantification of low affinity binding interactions between natural killer cell inhibitory receptors and targeting ligands with a self-induced back-action actuated nanopore electrophoresis (sane) sensor," Nanotechnology 32(4), 045501 (2020).
- [11] Storm, A. J., Storm, C., Chen, J., Zandbergen, H., Joanny, J.-F., and Dekker, C., "Fast dna translocation through a solid-state nanopore," *Nano letters* 5(7), 1193–1197 (2005).
- [12] Saharia, J., Bandara, Y. N. D., Karawdeniya, B. I., Hammond, C., Alexandrakis, G., and Kim, M. J., "Modulation of electrophoresis, electroosmosis and diffusion for electrical transport of proteins through a solid-state nanopore," *RSC advances* 11(39), 24398–24409 (2021).
- [13] Zehtabi-Oskuie, A., Jiang, H., Cyr, B. R., Rennehan, D. W., Al-Balushi, A. A., and Gordon, R., "Double nanohole optical trapping: dynamics and protein-antibody co-trapping," *Lab on a Chip* **13**(13), 2563–2568 (2013).
- [14] Morton, J. J., "Electrical and optical properties of materials," (2009).
- [15] Ludwig, M., Witt, M. U., and von Klitzing, R., "Bridging the gap between two different scaling laws for structuring of liquids under geometrical confinement," *Advances in colloid and interface science* **269**, 270–276 (2019).
- [16] Neumeier, L., Quidant, R., and Chang, D. E., "Self-induced back-action optical trapping in nanophotonic systems," New Journal of Physics 17(12), 123008 (2015).